Energy Reports 6 (2020) 2309–2323

Contents lists available at ScienceDirect

Energy Reports

journal homepage: www.elsevier.com/locate/egyr

Comprehensive thermodynamic and operational optimization of a solar-assisted LiBr/water absorption refrigeration system

S. Sharifi [a], F. Nozad Heravi [b], R. Shirmohammadi [a,d], R. Ghasempour [a,*], F. Petrakopoulou [c], L.M. Romeo [d]

[a] Faculty of New Sciences & Technologies, University of Tehran, Tehran, Iran
[b] School of Mechanical Engineering, University of Tehran, Tehran, Iran
[c] Department of Thermal and Fluid Engineering, University Carlos III of Madrid, Madrid, Spain
[d] Escuela de Ingeniería y Arquitectura, Departamento de Ingeniería Mecánica, Universidad de Zaragoza, Campus Río Ebro, María de Luna 3, 50018 Zaragoza, Spain

ARTICLE INFO

Article history:
Received 12 April 2020
Received in revised form 25 July 2020
Accepted 15 August 2020
Available online xxxx

Keywords:
Optimization
Solar energy
Exergy
Absorption refrigeration system
NSGA II
GMDH

ABSTRACT

Absorption cooling systems have been investigated for many years due to their ability to use low-grade heat instead of electricity as the energy source. The aim of this work is to advance the performance of a single-effect Lithium bromide/water absorption cooling system. Taking the generator and evaporator temperatures as variables, the system is optimized to maximize exergetic and energetic efficiencies at different operational conditions using a multi-objective–multi-variable Genetic Algorithm. The Group Method of Data Handling neural network approach is adopted to derive correlations between the design variables and operational parameters. Finally, the system is coupled to evacuated tube solar collectors and compared to a similar system. The results reflect a maximum improvement in energetic and exergetic efficiencies of about 9.1% and 3.0%, respectively. This translates into savings of 187 dollars for every square meter of solar collector at present time. This improvement is achieved by decreasing the mean temperature of the generator by 6.2 °C and increasing the mean temperature of the evaporator by 1.6 °C. In the case of applying low-grade heat such as solar energy, it brings about both an improvement in the thermodynamic performances and a reduction in the generator temperature.

1. Introduction

Absorption cooling systems (ACSs) are conventional systems for air-conditioning and refrigeration that use thermal energy to produce cooling from low-grade heat sources such as solar energy and waste heat (Xu et al., 2015). In addition, ACSs use environmentally friendly working fluids that do not cause ozone depletion (Debnath et al., 2014). Because of these important reasons, many studies have developed methods to improve the performance of such systems (Ghorbani et al., 2018b). Thermodynamic analysis and optimization are the main methods of improving the performance (Misra et al., 2006; Kholghi and Mahmoudi, 2019).

Thermodynamic analyses are based on the first and second laws of thermodynamics (Ghorbani et al., 2019). The first law establishes the principle of energy conservation (the quantity of energy) (Mehrpooya et al., 2019). The coefficient of performance (COP) of a cooling system indicates its performance in terms of the first law. Likewise, the quality of energy is expressed by the second law (Dincer and Cengel, 2001). Exergy is defined as a combination of the first and second laws (Shirmohammadi et al., 2018) or more precisely, has the concepts of both the quantity and quality of energy (Petrakopoulou et al., 2012b). The exergetic efficiency (η_{Π}) demonstrates how much exergy has been destroyed due to the system's irreversibilities that also have an environmental impact. Thus, the exergetic efficiency can be another expression of efficiency in terms of the second law (Petrakopoulou et al., 2012a).

LiBr/water and water/ammonia are the most common working fluids in ACSs. However, LiBr/water is usually used for air-conditioning applications (Misenheimer and Terry, 2017). Many researchers have considered single-effect absorption cycles with LiBr/water as the working fluid from a thermodynamics point of view. Şencan et al. (2005) evaluated the exergy loss in each component, as well as the COP and η_{π} of the system. The conclusion was that η_{π} and COP have an inverse relation with the temperature of the heat source. The result of Kilic and Kaynakli's (2007) thermodynamic study on ACSs indicated that the COP increased overall, as the temperature increases in the evaporator

* Corresponding author.
E-mail address: Ghasempour.r@ut.ac.ir (R. Ghasempour).

https://doi.org/10.1016/j.egyr.2020.08.013

List of abbreviations

COP	coefficient of performance
$\dot{Q}$	heat transfer rate [kW]
$\dot{W}$	work rate [kW]
$\dot{m}$	mass flow rate [kg/s]
h	enthalpy (kJ/kg)
s	entropy (kJ/kg-K)
$\dot{I}$	exergy rate [kW]v
NPV	net present value
T	temperature [°C] or [K]
F	non-dimensionalization object
y	output variable
G_T	solar radiation
r_i	average inflation rate (%)
r_n	nominal annual escalation rate (%)
r_r	real annual escalation rate (%)
i	inflation rate (%)
k	escalation rate
T_{hot}	mean temperature of the heat source (°C)
T_{cold}	mean temperature of the stream to be cooled (°C)
FC	fuel cost
CDEC	carbon dioxide emissions cost

Greek letters

ψ	special exergy (kJ/kg)
η	efficiency
ε	heat exchanger effectiveness

Subscripts and superscripts

gen	generator
abs	absorber
eva	evaporator
cond	condenser
amb	ambient
opt	optimum
i	input
e	exit
o	output
0	reference state
II	second law
p	pump
col	collector
L	levelized
NG	natural gas
CO_2	carbon dioxide
n	years of operation

Acronyms

ACS	absorption cooling system
ETC	evacuated tube solar collector
HE	heat exchanger
GMDH	group method of data handling
GA	genetic algorithm
LCOC	levelized cost of cooling
CRF	capital recovery factor
ANN	artificial neural network

and generator, while the temperature decreases in the absorber and condenser. Another study, conducted by Kaynakli and Kilic (2007), concluded that a solution heat exchanger (HE) has more effect on COP, in comparison with a refrigerant HE. This effect can reach 44% on the COP, while the effect of the refrigerant HE is only 2.4%. Avanessian and Ameri (2014) investigated the influence of climatic conditions on the second law efficiency. Their results showed that ambient temperature has a direct effect on the total exergy efficiency. Another study on energy and exergy analyses, conducted by Modi et al. (2017), indicated that most of the exergy destruction is found in the generator and absorber, calculated 40% and 28%, respectively.

Improving the performance of single-effect ACSs requires optimizing desired objectives. By analyzing ACSs thermodynamically, Gomri (2009) concluded that there is an optimum temperature for the generator, condenser, and evaporator at which the COP and the exergetic efficiency are maximum. In another study conducted by Gomri (2013a), a simulation of a single-effect ACS using solar and natural gas as energy sources was undertaken. He found that an optimum generator temperature is derived at a specific condenser temperature. This generator temperature is pivotal as it requires the smallest number of solar collectors and yields the maximum COP and exergetic efficiency. These two studies report that there can be a generator temperature in which both the COP and the exergetic efficiency are at their maximums. However, by optimizing the single-effect ACSs from energetic and exergetic points of view, in the present study and in other studies (Samanta and Basu, 2016), it is seen that the maximum COP and exergetic efficiency are achieved at different generator temperatures for the same condenser temperature. Not correct optimization and the specification of such conditions limit the cited studies.

Application of thermodynamic principles to realize optimization has been carried out in many studies with the goal to find the conditions under which both the COP and the exergetic efficiency are maximum. Samanta and Basu (2016) optimized a single effect ACS to maximize the COP and exergetic efficiency of an ACS system. They reported that there is an optimum generator temperature for any given combination of evaporator and condenser temperatures, which is lower than the generator temperature corresponding to the maximum COP. This finding is validated as we obtained similar results in our present study. The main differences in the methodology of the present study when compared to the study of Samanta and Basu are the following: First, the present study achieves optimum system mode by taking into account both the generator and evaporator temperatures, not just the generator temperature; second, the present study calculates a wide range of operational parameters that can affect the optimum mode and derives correlations that in turn yield the optimum generator and evaporator temperatures.

The latest research on the thermodynamic optimization of ACSs is mentioned below. Modi et al. (2017) investigated the effects of different parameters on a single-effect ACS and optimized the system for a specific condition to maximize the COP and exergetic efficiency. They concluded that the optimum generator temperature is before the corresponding generator temperature of the maximum COP and after the corresponding generator temperature of the maximum exergetic efficiency. In addition, COP and exergetic efficiency were in conflict with the evaporator temperature. Pandya et al. (2017) conducted a similar study. They indicated that the exergetic efficiency is more important for determining the optimum generator temperature in comparison to COP. Although a single-effect ACS has been optimized by considering COP and exergetic efficiency, the optimization was limited to specific operational conditions and generator temperatures. A lack of comprehensive studies on the thermodynamic optimization led the authors to identify the optimum mode of the

single-effect ACS for every operating condition, by considering generator and evaporator temperatures as the design variables.

Thermodynamic optimization has also been applied to other configurations of ACSs. Medjo Nouadje et al. (2016) investigated the optimization of a double-effect parallel flow ACS by considering the COP and exergetic efficiency of the system. They pointed out that the optimum mode of the system varies with varying temperatures of the main components. They assessed five optimum modes, which had different temperatures in the main components. Thermodynamic optimization for a double-effect series flow was also conducted by Ghani et al. (2017). They found a roughly 10.25% and 38.5% improvement in COP and exergetic efficiency by using optimum component temperatures. Another optimization, considering COP and exergetic efficiency, was carried out by Azhar and Siddiqui (2017). The optimization was carried out using specific evaporator, condenser, and absorber temperatures. It was observed that the lack of supporting studies documenting the thermodynamic optimization is also present in double-effect ACSs, as it was in single effect ACSs.

A large number of researchers have used the Group Method of Data Handling (GMDH) as a powerful tool with a high estimation capability to model and optimize proposed systems (Nasruddin et al., 2019). The GMDH method introduced by Ivakhnenko (Farlow, 1981) has been used to achieve many different goals, such as predicting, modeling, and optimizing thermal systems. Moreover, the GMDH possesses the ability to obtain implicit expressions for the relationship between input and output data. Sohani et al. Teng et al. (2017) used five soft computing and statistical tools, including artificial neural networks (ANN) and GMDH, in the performance analysis of desiccant-enhanced evaporative cooling systems. As a result, they mentioned that GMDH has a decent capability for evaluating the performance of the system. In another study, Jafarian et al. (2017) used GMDH to model and optimize dew-point evaporation coolers. They stated that their proposed GMDH-type model yields the simple equations, which can be used by designers, engineers, or researchers, independently from the network structure or its input data. Shirmohammadi et al. (2015) optimized mixed refrigerant systems in low-temperature applications using GMDH along with genetic algorithm. They found that their proposed model has advantages in quantifying the consumed power of cascade refrigeration cycles over nonlinear programming techniques.

Applications of hybrid solar energy systems have been growing (Ghorbani et al., 2020). Being the most abundant and free form of energy in many regions, solar energy would be an appropriate option for combining renewable energies with ACSs, particularly for domestic applications (Ali, 2017). Ali et al. (2008) appraised the performance of using the single-effect LiBr/water ACS for a floor area of 270 m^2 in Oberhausen, Germany. The conclusion was that a 4.23 m^2 evacuated tube solar collector (ETC) is needed for supplying 1 kW of cooling load. A prototype was tested by Izquierdo et al. (2014) in Madrid, Spain, to meet the seasonal cooling demand of a laboratory with single- and double-effect ACSs, as well as 48 m^2 flat plate solar collectors. The authors concluded that solar energy alone is sufficient to meet the operational temperature of the single-effect mode of the prototype. Nevertheless, an external energy source may be necessary for the double-effect ACS, and the existence of a back-up system allows for a sustainable ACS in the event of solar energy disruption. Experimental and analytical analyses of Chen et al. (2017) study an air-cooled single-effect ACS combined with ETCs. They reported that with an average COP of about 0.61, the system was able to provide 65% of the total cooling load of the considered building.

As compared to previously mentioned reference studies, this study goes a step further by offering a new combination of objectives and variables in optimization and more importantly yields equations which can be used to create a model to achieve the outcome of any set of operational conditions. The present study zeroes in on the optimization of a single-effect LiBr/water ACS with a significant emphasis placed on using the first and second laws of thermodynamics. The study considers operational parameters, including temperatures of the condenser, absorber, and ambient, as well as the effectiveness of the HE. The first step towards fulfilling the aim of the study is modeling the system using MATLAB. After verifying the model, a Genetic Algorithm (GA) is applied to optimize the COP as well as η_π simultaneously and find their corresponding generator and evaporator temperatures for each set of operational parameters. This process is repeated to compile a database that included system performances in various operational conditions. Then, the equations showing the correlations between the operational parameters and the outputs (COP, η_π, generator temperature, and evaporator temperature) are derived using the GMDH neural network method. To summarize, the study yields a novel perspective on system optimization along with providing general equations for maximizing both energetic and exergetic efficiencies. Finally, the optimized model is compared to a similar one, in order to assess the improvement of the former. Similarly, novel points of the study are:

- The use of a multi-objective–multi-variable GA method to optimize the ACS by considering energetic and exergetic efficiencies as objectives and generator and evaporator temperatures as variables.
- The optimization is conducted on a wide range of operational parameters such as temperatures of condenser, absorber, and ambient, as well as the effectiveness of the HE.
- The correlations between objectives and operational parameters are found.

2. System description

A schematic of a single-effect ACS is shown in Fig. 1. The main components of an ACS are a condenser, a generator, an evaporator, an absorber, a solution HE, an expansion valve, a solution expansion valve, and a pump. The concentrated solution (concentrated by a refrigerant) is heated by a low-grade heat source in the generator, converting a portion of the refrigerant to steam. The diluted solution produced at the outlet of the generator is directed to the absorbent. The hot refrigerant vapor is condensed in the condenser and it then passes through the evaporator. The reduction in pressure through the expansion valve simplifies the vaporization of the refrigerant, which, in the end, absorbs the heat from the environment. The weak solution produced in the generator flows down through the solution expansion valve to the absorber. The refrigerant vapor produced in the evaporator comes to the absorber where it is absorbed by the weak solution, resulting in a strong solution. That solution is subsequently pumped by the solution pump to the generator, where it is heated, and the cycle is repeated [3].

3. System method

3.1. Simulation assumptions

Several assumptions are necessary to simulate the system (Bagheri et al., 2019):

- Steady conditions are assumed for simulations and analyses.
- The evaporator and the condenser outlet refrigerants are saturated vapor and liquid, respectively.

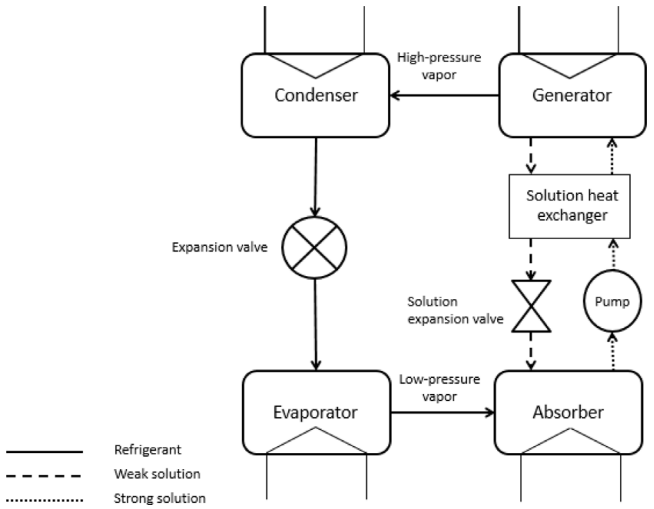

Fig. 1. Schematic of a single-effect ACS.

- The absorber and the generator outlet solutions are at equilibrium conditions at the corresponding temperatures.
- Pressure drops for all components and connecting pipes are considered negligible.
- Heat losses for all components and connecting pipes are considered negligible, unless otherwise stated.
- The temperature and pressure of the reference environment are the ambient temperature and 100 kPa, respectively.

3.2. Thermodynamic analysis

The application of the first and second laws of thermodynamics, as well as the principle of mass conservation, are needed for the thermodynamic analyses of the system (Kumar and Layek, 2019). Under steady-state conditions, the equations of overall mass and energy conservation, where both kinetic and potential energies are neglected, are as follows:

- Mass conservation

$$\sum \dot{m}_i = \sum \dot{m}_e \tag{1}$$

- Energy conservation

$$\sum \dot{Q} - \sum \dot{W} = \sum \dot{m}_e h_e - \sum \dot{m}_i h_i \tag{2}$$

For all parts of the system, Eqs. (1) and (2) are solved. The COP, representing the energy efficiency of the system, is expressed with Eq. (3):

$$COP = \frac{\dot{Q}_{eva}}{\dot{Q}_{gen} + \dot{W}_p} \tag{3}$$

Irreversibility, or exergy destruction rate, represented by İ, is analyzed based on the second law of thermodynamics. The equation of exergy destruction rate in a steady-state process is presented with Eq. (4) (Fratzscher, 1997):

$$\dot{I} = \sum \dot{m}_i \psi_i - \sum \dot{m}_e \psi_e + \sum \dot{Q}_i (1 - \frac{T_0}{T_i}) - \sum \dot{W} \tag{4}$$

Here, the definition of the exergy destruction rate for a control volume is an algebraic summation of amounts of exergy of streams, heat transfer rates from the environment at T_o towards the region at T_i temperature, and the work transfer to or from the control volume (Shirmohammadi et al., 2018). The specific exergy is calculated with Eq. (5).

$$\psi = (h - h_0) - T_0(s - s_0) \tag{5}$$

The exergetic efficiency represents the performance of the second law (Bejan et al., 1996):

$$\eta_{II} = \frac{\dot{Q}_{eva} \left| (1 - \frac{T_0}{T_{cold}}) \right|}{\dot{Q}_{gen}(1 - \frac{T_0}{T_{hot}}) + \dot{W}_p} \times 100 \tag{6}$$

The model of the single-effect ACS using LiBr/water as the working fluid is developed in MATLAB. The model includes the properties of LiBr/water taken from Klomfar and Patek studies (Pátek and Klomfar, 2006; Klomfar and Pa, 2009).

3.3. Optimization

There are numerous calculus-based methods used to derive local minimums. Despite the extensive use of such methods, there are some drawbacks, like a high dependency on initial guesses and finding local minimums rather than global ones (Arora, 2012). Thus, other optimization approaches like GAs are adopted. In contrast to traditional methods that use a single point in the search space, nature-inspired methods, such as GAs, make use of a set of solutions, avoiding the local minimum trap (Besarati et al., 2010).

There is another type of optimization, in which several objective functions represented as an objective vector, often conflicting with each other, are optimized, simultaneously. In this type of problem, there is not often a unique solution in which all objective functions achieve their optimal values, concurrently. Instead, a set of optimal solutions, the so-called Pareto optimal solutions, are achieved.

As Deb et al. (2002) reported, the improved version of NSGA, also known as NSGA-II, has the ability to maintain a better spread of solutions. In comparison with other elitist multi-objective evolutionary algorithms, it shows better convergence in obtaining a non-dominated front. To ensure that the optimal result is a global minimum, the diversity of GA algorithm solutions must be maintained (Besarati et al., 2010). Therefore, in this study, the NSGA-II algorithm is used in the optimization process.

Pareto optimal solutions properly demonstrate the different nature of single-objective and multi-objective optimization problems. A Pareto frontier, a space of objective functions in multi-objective problems, presents a set of solutions that although they have no superiority to each other, they are superior to the other solutions in the search space (Goldberg and David, 1989). It is clear that changing the design variables related to these non-dominant solutions cannot improve all of the objectives simultaneously. Such changes might improve one objective function but may end up deteriorating other ones. The inherent parallelism of evolutionary algorithms makes them a proper method for multi-objective optimization problems.

As shown in Figs. 2 and 3, even though the COP has a direct relationship with the evaporator temperature, the η_π decreases as the evaporator temperature increases. Moreover, the maximum points of COP and η_π at the corresponding evaporator temperature occur at different generator temperatures. Therefore, mindful of the conflict between COP and η_{II}, they are considered as our proposed objectives. If COP were adopted as the only objective, the generator temperature would increase substantially. Likewise, if the exergetic efficiency were adopted as the only objective, the COP would be out of a normal range. By adopting both COP and η_π as our objectives, not only will the generator temperature be within a proper range, but also a balance will be achieved between the COP and exergetic efficiency. As discussed before, GAs are proper methods to tackle optimization problems due to their superiority over calculus-based methods. Since the NSGA-II algorithm shows an excellent ability to maintain diversity in the population of design variables (Deb et al., 2002), it is used in the present study.

Table 1
Comparison between single and multi-objective optimizations.

System parameters	Single-objective optimization (COP)	Single-objective optimization (η_{II})	Multi-objective optimization (COP and η_{II})
COP	0.804	0.702	0.775
η_{II}	0.075	0.206	0.164
Generator temperature (°C)	83.59	88.08	84.78
Evaporator temperature (°C)	15	5	10.5

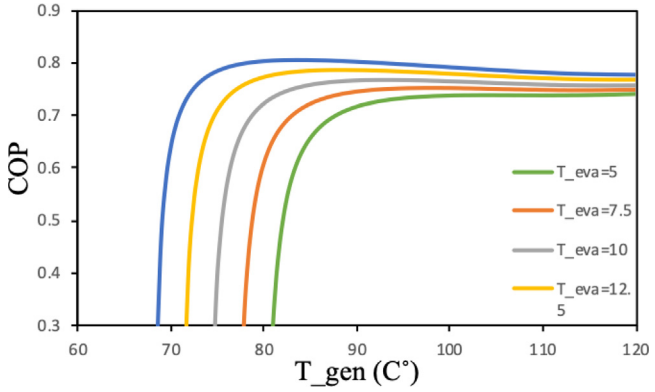

Fig. 2. The relationship of COP with T_{gen} and T_{eva}.

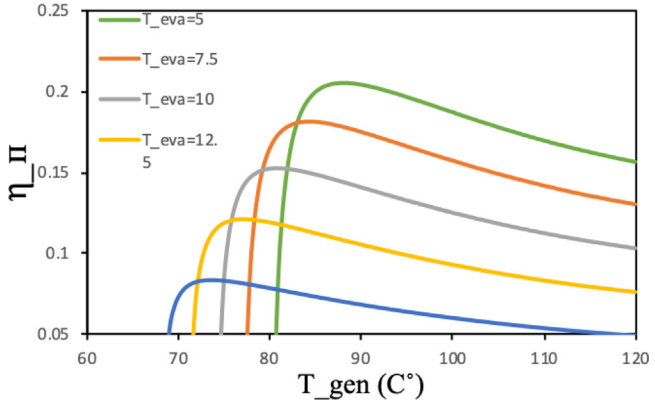

Fig. 3. The relationship of η_{π} with T_{gen} and T_{eva}.

The purpose of the optimization utilized in the present study can be explained by the data represented in Table 1. The data shows that by adopting single-objective optimization two efficiency values are obtained, one being of maximum value whereas the other being of low value. Indeed, the maximum COP occurs when the evaporator temperature is at the highest range, causing η_{II} to be in the low value. In contrast, the maximum of η_{II} occurs when the evaporator temperature is at the lowest range, causing COP to be in low value. However, by applying multi-objective optimization, which considers both COP and η_{II} as its objectives, both COP and η_{II} are closer to their maximums. In addition, the generator temperature in multi-objective optimization occurs relatively in low range.

It is noteworthy to mention that a cost analysis is not considered as an objective here. The cost analysis entails changing the size or quality of any given system. Furthermore, in cost analysis, the system has a specific scale and operates under specific working conditions (Seshadri, 1996). In operational optimization, only the generator and evaporator temperatures are adopted as variables. In this way, the system can be optimized regardless of its scale (Petela et al., 2017).

Table 2
Constants of Eq. (7) for LiBr/water working fluid (Saravanan and Maiya, 1998).

a	b	c	d
−232.32389209	217.76489634	201.5643421	4.17105216E−06

Table 3
GA optimization parameters.

Parameter	Value
Population size	150
Maximum number of generations	1000
Crossover fraction	0.9
Crossover function	Arithmetic
Pareto frontier population fraction	0.7
Tournament size	5
Function tolerance	1e-6

3.3.1. Genetic algorithm

GA optimization consists of several parts, i.e., initialization, fitness assignment, selection, crossover, and mutation. The purpose of the whole process is to optimize (i.e., minimize or maximize) specific objectives according to selected design variables (Ghorbani et al., 2018a). As seen in Fig. 4, after defining the operational condition and generating an initial population, the fitness values of each member of the population are evaluated. According to these fitness values, the population is ranked non-dominantly so that in each iteration of the GA, selection, crossover, and mutation take place, and the children population is obtained. After combining the parent and children populations, as well as ranking them using their fitness values, a new population is created from their combination. This process is repeated until a final criterion is satisfied.

In this study, the generator and evaporator temperatures are chosen as design variables and the energetic and exergetic (COP) efficiencies as the objectives. Often, optimizations include some equality or inequality constraints for their design variables. A nonlinear inequality constraint, Eq. (7), presented by Saravanan and Maiya (1998) that defines the allowed minimum generator temperature range based on operational conditions is used.

$$T_{gen} \geq a + \left(\frac{T_{cond}}{T_{eva}}\right) b + \left(\frac{T_{abs}}{T_{eva}}\right) c + (T_{cond} T_{abs} T_{eva})\, d \tag{7}$$

where, T_{cond}, T_{abs}, and T_{eva} are the condenser, absorber, and evaporator temperatures, respectively. The constants of Eq. (7) for LiBr/water working fluid are listed in Table 2. The GA optimization parameters are presented in Table 3.

3.3.2. Decision-making in multi-objective optimization

After obtaining the optimal design variables for a variety of operational conditions, a set of non-dominated solutions in the search space is obtained. Therefore, selecting a single final optimum point among the available optimum solutions strongly depends on the priorities of designers. However, as a basic method, a solution with the minimum distance from an ideal point in the search space can be chosen. The ideal point in the Pareto frontier is the point on which each objective is optimized regardless of satisfying other objectives. Since the proposed objectives may have different dimensions, a decision-making method

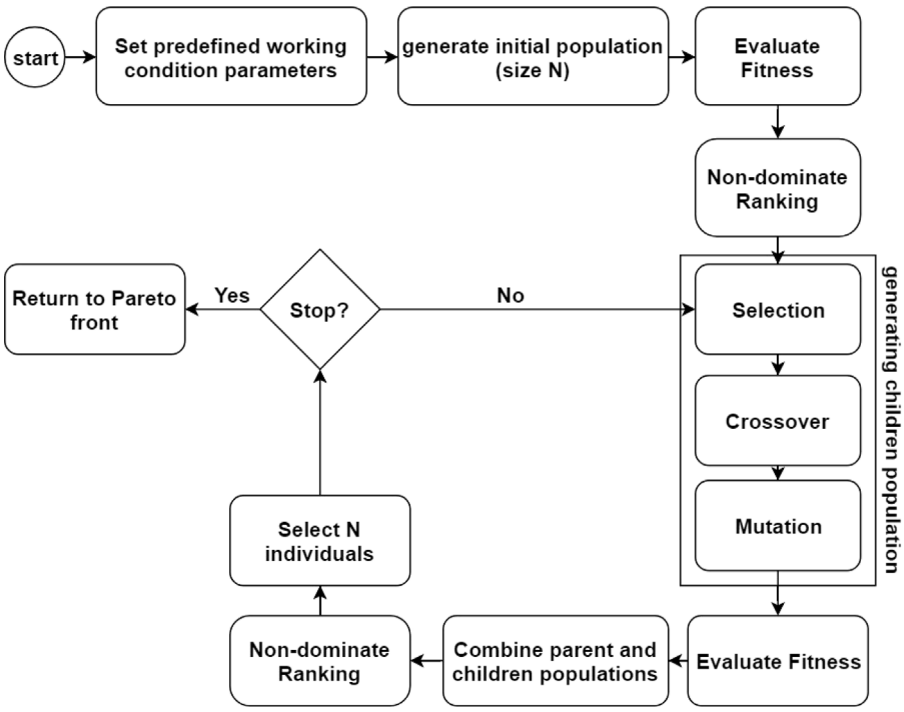

Fig. 4. The flowchart of NSGA-II algorithm for optimizing a single-effect ACS.

should be applied to make non-dimensional objectives before the decision-making procedure (Davarpanah et al., 2019). In this study, the Euclidian non-dimensionalization method is used for this purpose (Ahmadi et al., 2013).

In the Euclidian non-dimensionalization method, the definition of a non-dimensionalization object F_{ij}^{n} is as follows:

The selected solution has a minimum distance from the ideal point. The deviation of solutions of the Pareto frontier from the ideal point, denoted by d_{i+}, is calculated using the following equation:

$$d_{i+} = \sqrt{\sum_{j=1}^{n} F_{ij} - F_j^{ideal}} \tag{8}$$

In which n is the number of objectives, i is an index of each solution on the Pareto frontier ($i = 1, 2 \ldots, m$), and F_j^{ideal} is the ideal value calculated for the j_{th} objective. Therefore, the solution is selected by finding the minimum value of d_{i+}:

$$i_{final} = i \in \min(\mathrm{d}_{i+}); \quad i = 1, 2, \ldots, m \tag{9}$$

where i is the index of the final solution.

3.4. System modeling using the GMDH method

High estimation capability to model and optimize systems has led many researchers to use GMDH neural networks (Romeo and Gareta, 2006). The GMDH method has three main advantages over artificial neural network (ANN) methods. First, the GMDH method can derive explicit outputs that can be used in optimal system design processes, while ANN methods just provide implicit models like black boxes. Secondly, the GMDH method is a self-organized network i.e., it optimizes its structure according to data input. Lastly, by objectively selecting models of optimal complexity, the GMDH method avoids the overfitting problem often arising in ANN methods (Teng et al., 2017).

After creating a database, the GMDH method is used to model relationships between operational conditions and design variables. A set of operational conditions consists of different operational parameters, i.e., the condenser, absorber, and ambient temperatures, as well as the effectiveness of HE, are selected in their appropriate ranges randomly, and the GA algorithm is applied for each condition. Table 4 shows the ranges of these operational parameters.

Table 4
The operational parameters with their allowed ranges.

Operational parameters	T_{cond} (°C)	T_{abs} (°C)	T_{amb} (°C)	ε
Allowed range	25–45	25–45	20–40	0.5-0.9

The obtained database consists of operational parameters and their corresponding optimal values of COP, exergetic efficiency, and generator and evaporator temperatures. Because of the nonlinearity of the system and the complex relationships among used parameters, the GMDH method is used to obtain correlations among the parameters. The generator and evaporator temperatures are proposed as the outputs of the GMDH, and the operational parameters are as its input variables. The functions having the ability to calculate the optimal generator and evaporator temperatures for every LiBr/H_2O single-effect ACS's operational condition are found using the GMDH method.

The GMDH method is similar to a network of layers that contains many neurons with predefined functions. Fig. 5 shows a GMDH structure in which a, b, c, and d represent the network input parameters, and y stands for the network output. Each combination of any two input parameters forms a neuron in the next layer. The a and b inputs, for instance, form the ab neuron in the first hidden layer. After creating whole neurons in a layer, neurons with more accurate outputs are selected according to a predefined threshold. The selected neurons, forming neurons of the next layer, are shown in green color in Fig. 5. In order to calculate the accurate output of these correlations, a proper number of hidden neurons inside the neural network, depending on the complexity and nonlinearity of correlations between the input and output data, are required. The base algorithm of the GMDH is a procedure of constructing a high-order polynomial for an output variable, y_i, in terms of m input variables. In this

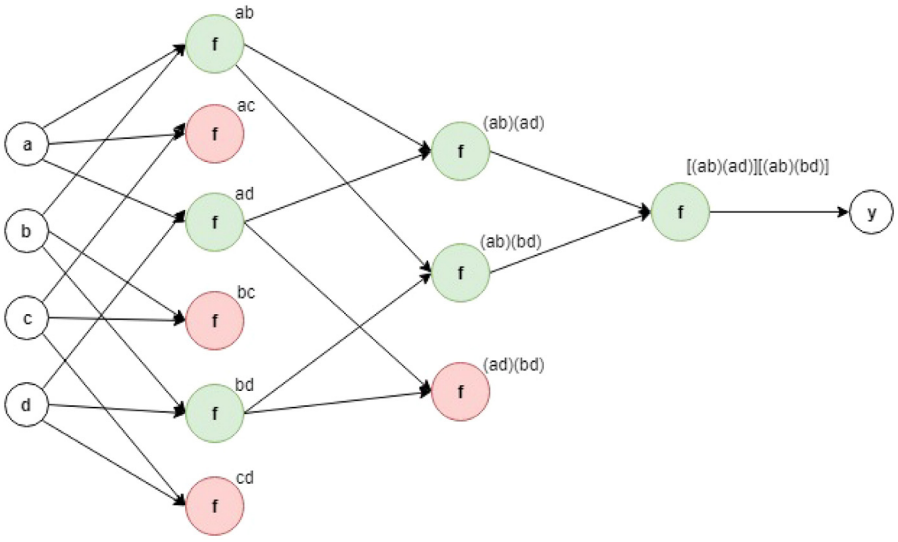

Fig. 5. The GMDH structure.

procedure, the constants in polynomials are optimized in order to minimize the error between the actual y_i and the estimated value, $\hat{y}_i$ (Ghorbani et al., 2016). In this study, three different functions are selected as the function of the GMDH neurons, presented in Eqs. (10)–(12).

$$f_1(x_i, x_j) = a_0 + a_1 x_i + a_2 x_j + a_3 x_i x_j \tag{10}$$

$$f_2(x_i, x_j) = a_0 + a_1 x_i^2 + a_2 x_j^2 + a_3 x_i x_j \tag{11}$$

$$f_3(x_i, x_j) = a_0 + a_1 \sqrt{x_i} + a_2 \sqrt{x_j} + a_3 x_i x_j \tag{12}$$

The output of the GMDH was $\hat{f}$ function, which gives the output value, $\hat{y}_i$, with regard to correlated inputs, $X = (x_{i1}, x_{i2}, \ldots, x_{in})$, as an estimation of the actual y_i value. There are M pair data as follows:

$$y_i = f(x_{i1}, x_{i2}, \ldots, x_{in}) \quad (i = 1, 2, \ldots, M) \tag{13}$$

The GMDH neural network is trained using this data, and the network output $\hat{y}_i$ is obtained as described below:

$$\hat{y}_i = \hat{f}(x_{i1}, x_{i2}, \ldots, x_{in}) \quad (i = 1, 2, \ldots, M) \tag{14}$$

In this step, the constants of neurons' function are optimized in order to minimize the error squares between all data pairs and their corresponding GMDH outputs. This error square is expressed with Eq. (15). The least square logic is used to find the optimum values of these constants.

$$E = \frac{\sum_{i=1}^{M} (y_i - \hat{y}_i)^2}{M} \tag{15}$$

In the GMDH training process, the contributions of data for training and testing of the GMDH model are 80% and 20%, respectively. After the formation of the GMDH network and considering the structure of the network inversely, a correlation between the considered output and inputs are obtained. In Fig. 6, it is observed that the GMDH model receives the condenser, absorber, and ambient temperatures, as well as the effectiveness of HE as its inputs and outputs the optimum generator and evaporator temperatures. By having the inputs and outputs, the optimum COP and exergetic efficiency are calculated.

3.4.1. Different criteria for evaluation of the GMDH model

Different criteria can be used to evaluate the trained GMDH neural network. The coefficient of determination (R^2), the variance accounted for (VAF), and the correlation factor (CF), which

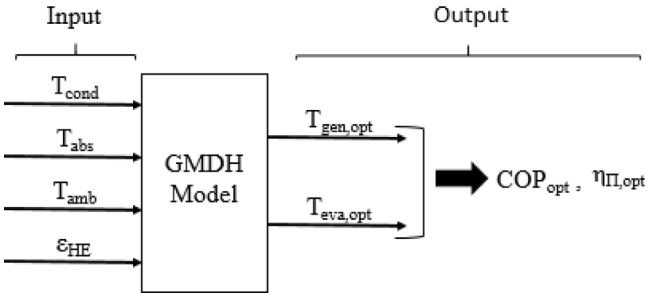

Fig. 6. The schematic of the GMDH model and its inputs and outputs.

are calculated using Eqs. (16)–(18).

$$R^2 = 1 - \frac{\sum_{i=1}^{M} (y_{i,act} - y_{i,gmdh})^2}{\sum_{i=1}^{M} (y_{i,act} - \bar{y}_{i,gmdh})^2} \tag{16}$$

$$VAF\% = \left(1 - \frac{VAR\{y_{i,act} - y_{i,gmdh} | i = 1, 2, \ldots, M\}}{VAR\{y_{i,act} | i = 1, 2, \ldots, M\}}\right) \times 100 \tag{17}$$

$$CF = \frac{\sum_{i=1}^{M} (y_{i,act} - \bar{y}_{i,act}) \times (y_{i,gmdh} - \bar{y}_{i,gmdh})}{\sqrt{\sum_{i=1}^{M} (y_{i,act} - \bar{y}_{i,act})^2 \times \sum_{i=1}^{M} (y_{i,gmdh} - \bar{y}_{i,gmdh})^2}} \tag{18}$$

where, M is the number of sample data, $y_{i,act}$ is the actual output of each data set, $y_{i,gmdh}$ is the corresponding estimated value using the GMDH trained network, and $\bar{y}_{i,act}$ and $\bar{y}_{i,gmdh}$ are the average values of actual and predicted outputs, respectively. In a well-trained network, lower values of R^2 and CF represent a better correlation between inputs and output. Moreover, the VAF should be close to 100% to have a better convergence between the estimated and actual values (Ziari et al., 2015).

3.5. Sensitivity analysis

Sensitivity analysis is beneficial for designers because it shows the effects of input variation on the output of the system (Florides et al., 2003). The sensitivity can be expressed analytically with Eq. (19), showing the dependency of system characteristics on the variation of a particular input parameter.

$$S = \left(\frac{\frac{\Delta Y}{Y}}{\frac{\Delta X}{X}}\right)_r \tag{19}$$

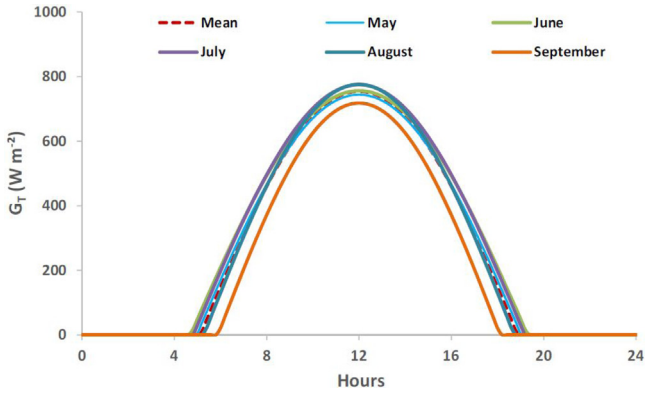

Fig. 7. The incident solar irradiation on the collector during different days for Athens.

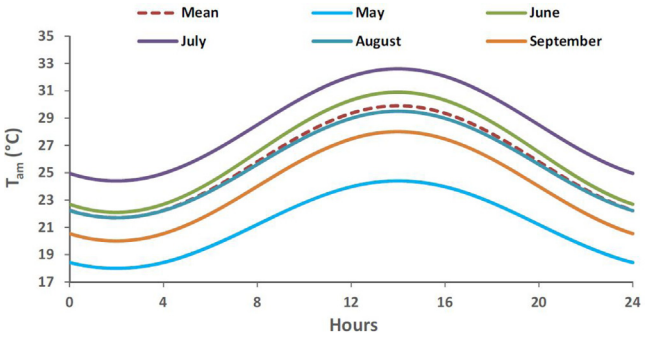

Fig. 8. The ambient temperature during different days for Athens.

In this equation, X is an input parameter, Y is a system characteristic, and the subscript r stands for reference point. In the present study, the reference point was an operational condition with values that are in the middle of determined ranges, i.e., 35 °C for ambient and absorber temperatures, 30 °C for the condenser temperature, and 0.7 for the effectiveness of the heat exchanger.

3.6. Solar analysis

In order to compare the performance of the obtained optimum mode of the ACS with the results of Bellos et al. (2017), similar underlying assumptions are made when evaluating this section. Similarly, an ETC type of a solar collector is selected with efficiency determined with the following equation (Kalogirou, 2003):

$$\eta_{th} = 0.82 - 2.19\left(\frac{T_{col,i} - T_{amb}}{G_T}\right) \tag{20}$$

As in Bellos et al. weather data from Athens, Greece, are assumed here as well. The data for average daily incident solar irradiation on the collector and ambient temperature is depicted in Figs. 7 and 8, respectively. These data were collected in five warm months, and the mean daily temperature of the months was selected as representative for this period.

3.7. Cost analysis

3.7.1. Fuel cost

Adjusting the generator and evaporator temperatures in the present study affect the performance of the system without any changes in the system. The capital investment and operating and maintenance costs are assumed to be the same as those of Bellos et al. (2017). Cost savings are calculated from the economic differences of cooling loads between this study and that of Bellos et al. To calculate the cost savings, it is assumed that an auxiliary heater using natural gas compensates for the extra energy providing the cooling load difference. The levelized annual fuel cost associated with the consumption of natural gas in the auxiliary heater is obtained as follows (Seshadri, 1996):

$$FC_{L,NG} = FC_{0,NG}\frac{k_{NG}(1-k_{NG}^{n})}{(1-k_{NG})}CRF \tag{21}$$

where, $FC_{0,NG}$ is the consumption of natural gas in the first year of operation, and n is the years of operation, considered here 20. To calculate the $FC_{0,NG}$, 1m^3 of natural gas is considered to be equal to 3723 kJ and 35.31 cents, and the efficiency of the auxiliary heater is assumed to be 0.85 (Gomri, 2013b). The capital recovery factor (CRF) is calculated as (Seshadri, 1996):

$$CRF = \frac{i(1+i)^{n}}{(1+i)^{n}-1} \tag{22}$$

Moreover, K_{NG}, the escalation rate of the price of natural gas, can be calculated as:

$$K_{NG} = \frac{1+r_{n,NG}}{1+i} \tag{23}$$

where,

$$(1+r_{n,NG}) = (1+r_{r,NG})(1+r_i) \tag{24}$$

where i is the average interest rate, $r_{n,NG}$ is the annual nominal escalation rate, $r_{r,NG}$ is the real escalation rate of the price of natural gas, and r_i is the inflation rate. Table 5 shows the values of these parameters.

3.7.2. Cost of carbon dioxide emissions

Carbon dioxide emissions affect the environment and human health, imposing indirect costs, assessed here as a part of the costs

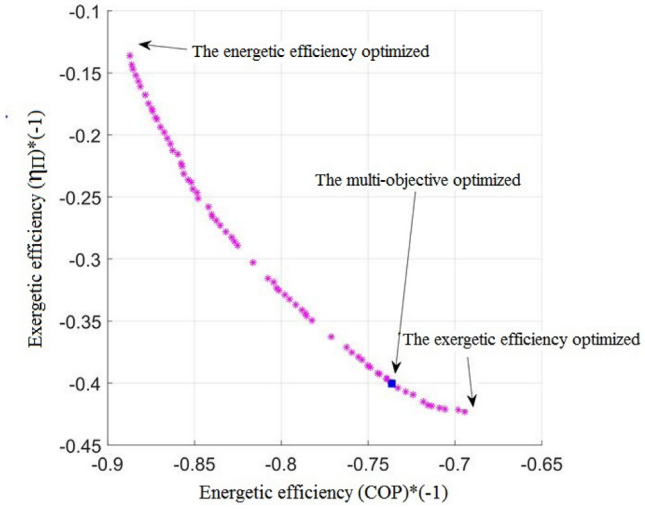

Fig. 9. The Pareto frontier of the single-effect ACS for a specific operational condition.

Table 5
Input parameters of the economic analysis (Shirazi et al., 2016).

Parameter	Value
Average inflation rate (r_i)	2.9 (%)
Interest (discount) rate (i)	6 (%)
Real escalation rate of natural gas price ($r_{r,NG}$)	2 (%)
Real escalation rate of carbon dioxide emission price ($r_{r,CO2}$)	2.04 (%)

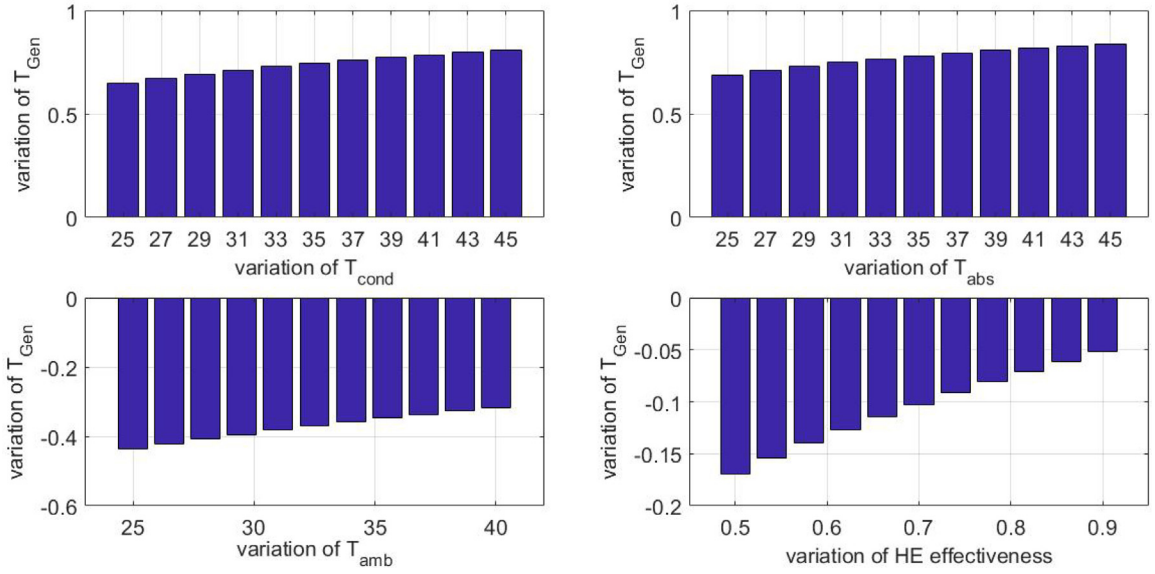

Fig. 10. Sensitivity analysis for the generator temperature of the single-effect ACS.

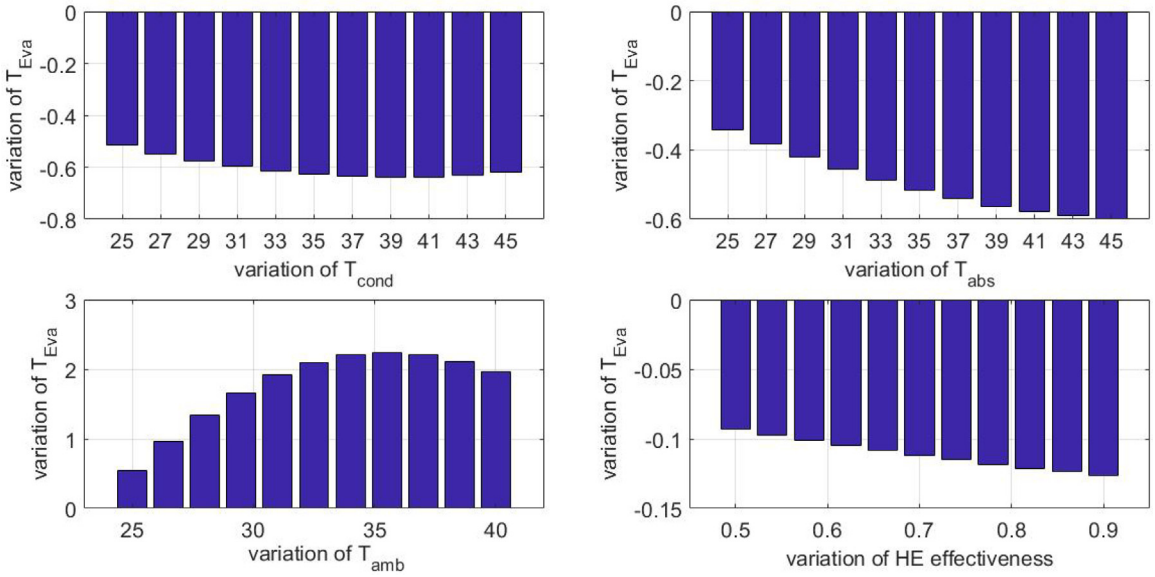

Fig. 11. Sensitivity analysis of the evaporator temperature of the single-effect ACS.

of the system. The cost of carbon dioxide emissions of natural gas is evaluated using the same process as for calculating the fuel cost (Seshadri, 1996).

$$CDEC_{L,CO_2} = CDEC_{0,CO_2}\frac{k_{CO_2}(1-k_{CO_2}^{n})}{(1-k_{CO_2})}CRF \tag{25}$$

where, $CDEC_{0,CO_2}$ is the carbon dioxide emissions of natural gas in the first year of operation and k_{CO_2} is obtained from the same process as K_{NG}, using the corresponding nominal escalation rate for carbon dioxide emissions (r_{n,CO_2}) shown in Table 5. To calculate the $CDEC_{0,CO_2}$, it is assumed that $1m^3$ of natural gas releases 1.8564 kg CO_2 (Gomri, 2013b) with a removal cost of 0.2667 cents per kg of CO_2 (Sokhansefat et al., 2018).

Additionally, the present value of the total cost over the years of operation is calculated as (Seshadri, 1996):

$$NPV_{T,NG} = \frac{FC_{L,NG} + CDEC_{L,CO_2}}{CRF} \tag{26}$$

4. Results and discussion

4.1. Verification of the thermodynamic model of the single-effect ACS

For the validation process, the results of this study are compared to the results of (Kaushik and Arora, 2009). Table 6 illustrates the details of the validation. It is observed that the difference between the results of the presented study and that of Kaushik and Arora is small (Kaushik and Arora, 2009).

4.2. Optimization

After the simulation of the cycle, the optimization using the GA method follows. The outputs of the optimization are Pareto frontiers, in which optimum solutions are in a range of our objectives for each set of operational parameters. It is noteworthy to mention that the numbers in Pareto frontiers are negative, since the GA method finds local minimums. Therefore, to find

Table 6
Comparison of energy and exergy efficiencies between (Kaushik and Arora, 2009) and the present study.

T_{cond} (°C)	T_{abs} (°C)	T_{eva} (°C)	T_{gen} (°C)	η_{II} Kaushik and Arora (2009) (–)	η_{II} present study (-)	Deviation from Kaushik and Arora (2009) (–)	COP Kaushik and Arora (2009) (–)	COP present study (–)	Deviation from Kaushik and Arora (2009) (%)
40	40	7.2	85	0.1187	0.1209	1.8534	0.7173	0.7163	0.1394
37.8	37.8	7.2	80	0.1318	0.1338	1.5174	0.7340	0.7331	0.1226
35	35	7.2	75	0.1496	0.1523	1.8048	0.7668	0.7655	0.1695
30	30	7.2	70	0.1778	0.1797	1.0686	0.8243	0.8189	0.6551
40	40	7.2	90	0.1157	0.1168	0.9507	0.7428	0.7421	0.0942
37.8	37.8	7.2	85	0.1260	0.1278	1.4285	0.7578	0.7572	0.0791
35	35	7.2	80	0.1397	0.1422	1.7895	0.7797	0.7796	0.0128
30	30	7.2	75	0.1598	0.1624	1.6270	0.8161	0.8162	0.0122
37.8	37.8	4	87.5	0.1672	0.1696	1.4354	0.7285	0.7302	0.2333
37.8	37.8	6	87.5	0.1396	0.1417	1.5042	0.7494	0.7508	0.1868
37.8	37.8	8	87.5	0.1105	0.1119	1.2669	0.7583	0.7676	1.2264

the maximum objectives, we need to find the minimum of the reverse objectives. The final optimum point is selected among the available optimum solutions. Fig. 9 shows a Pareto frontier and its selected optimum point for a specific operational condition. By repeating this process for various operational conditions, a data set is achieved and used for estimating the correlations by utilizing the GMDH method.

4.3. The GMDH method

A thermodynamically optimized model is obtained using the GMDH method trained with the set of data achieved from the previous stage. Table 7 shows the different criteria for the GMDH model with three neuronal functions and three number of layers for each output. It should be noted that the optimization was performed to maximize the energetic and exergetic efficiencies by varying the generator and evaporator temperatures. Thus, the outputs represent not only the energetic and exergetic efficiencies but also the corresponding generator and evaporator temperatures. As shown in Table 7, all criteria for all correlations are in acceptable ranges, the values of R^2 and CF are close to each other, and the VAF values approached 100%. Accordingly, the relationship among the parameters is well correlated. The models that have the maximum R^2 are selected for the next analyses (the rows highlighted green). Since the criteria are very close to each other, it cannot be claimed precisely which functions or how many layers are appropriate using the GMDH approach.

4.4. Sensitivity analysis

The sensitivity analysis shows how much the system inputs can affect its outputs. For the optimum generator temperature, Fig. 10 shows that the most effective parameters are the absorber and condenser temperatures that have a direct relationship with the optimum generator temperature. In addition, the sensitivity increases at higher temperatures of both the absorber and the condenser. The effectiveness of the HE and the ambient temperature have an inverse relation with the optimum generator temperature. Specifically, HE effectiveness has the least impact on the optimum generator temperature.

The most effective parameter for the optimum evaporator temperature is the ambient temperature (as shown in Fig. 11). In contrast to the optimum generator temperature, the absorber and condenser temperatures have inverse relations with the optimum evaporator temperature. Additionally, it is observed that the absorber and condenser temperatures have almost the same effect on the generator temperature.

The influence of operational parameters on the COP and η_{II} are demonstrated in Figs. 12 and 13, respectively. As it was expected, increasing the absorber and condenser temperatures decreases both outputs. However, the effect of the COP and η_{II} on the absorber temperature is slightly higher than that of the condenser temperature. The reason for this is that the ambient temperature and not the reference temperature is used in the η_{π} equation. As both the COP and η_{II} are considered for selecting the optimum points, all of the outputs are affected by the ambient temperature. Therefore, it follows that the most influential parameter for η_{II} is the ambient temperature. The HE effectiveness has minimal effect on both outputs; however, it has a higher effect on the η_{II}.

4.5. Comparative investigation of the proposed model

In this section, the results of the combination of the optimized ACS with ETCs are compared to those of Bellos et al. (2017) (particularly, the analyses performed between 10:00 to 16:00). The comparison between the COP and η_{II} of the optimized ACS with the same parameters used in the study of Bellos et al. (2017) are illustrated in Figs. 14 and 15, respectively. The mean of both the COP and η_{II} for the present study are found to be higher than those of Bellos et al. (2017). The differences between the means are about 3.6% and 0.6% for the COP and η_{II}, respectively. It is important to state that when compared to the Bellos et al. study that included an exergetic optimization, the found improvement in the exergetic efficiency is rather small. In Bellos et al. (2017) study, the study design was such that exergetic efficiency was innately built into the process from the outset. Bellos et al. (2017) study design was primarily designed to optimize only one objective, namely, exergetic efficiency; whereas, the present study design was endeavored to optimize multiple objectives, both exergetic and energetic efficiencies. Furthermore, the maximum difference is about 9.1% and 3.0% for the COP and η_{II}, respectively. As it is assumed that by increasing the T_{amb}, both T_{cond} and T_{abs} increase, until 14:00 (that T_{amb} increases) the COP decreases. However, η_{II} increases with increasing T_{amb}. Thus, the behavior of the optimized system proves the results of the sensitivity analyses discussed in the previous section.

It is demonstrated that the optimized model regulates its outputs (COP and η_{II}) by varying both the evaporator and generator temperatures. As also reflected in Figs. 16 and 17 below, the results are in contrast to conventional expectations.

Fig. 16 illustrates the comparison between the T_{gen} of the optimized ACS in the present study and that of Bellos et al. (2017). The comparison indicates that T_{gen} of the optimized ACS is 6.9% (6.2 °C) lower than that of (Bellos et al., 2017) on average. As the T_{amb} becomes higher, the difference between the T_{gen} of optimized ACS and that of Bellos et al. (2017) increases, reaching a difference of 8.3 °C. It is a unique feature of the optimized ACS that it does not only operate at lower T_{gen}, but it also has higher COP and η_{II}. In the case of a solar ACS, it is suggested that the

Table 7
Different criteria for the GMDH model of the single-effect ACS.

Output	Layer	Function	R^2	VAF%	CF	Output	Layer	Function	R^2	VAF%	CF
T_{gen}	2 Layers	f1	0.9390	93.9016	0.9691	T_{eva}	2 Layers	f1	0.9131	91.3339	0.9560
		f2	0.9478	94.8888	0.9743			f2	0.8998	89.9991	0.9488
		f3	0.9508	95.1022	0.9754			f3	0.9278	93.2188	0.9659
	3 Layers	f1	0.9464	94.6425	0.9730		3 Layers	f1	0.9035	90.3997	0.9509
		f2	0.9436	94.6263	0.9731			f2	0.9183	92.0537	0.9595
		f3	0.9381	93.8380	0.9688			f3	0.9275	92.7514	0.9633
	4 Layers	f1	0.9464	94.6468	0.9729		4 Layers	f1	0.9434	94.4476	0.9719
		f2	0.9520	95.1995	0.9758			f2	0.9417	94.2008	0.9707
		f3	0.9543	95.4325	0.9769			f3	0.9306	93.2752	0.9662
COP	2 Layers	f1	0.9041	90.4203	0.9510	η_{II}	2 Layers	f1	0.9376	93.8455	0.9688
		f2	0.9039	90.3849	0.9507			f2	0.9584	95.8623	0.9793
		f3	0.9055	90.6409	0.9521			f3	0.9659	96.6027	0.9829
	3 Layers	f1	0.9136	91.3602	0.9560		3 Layers	f1	0.9770	97.7006	0.9885
		f2	0.9068	90.7334	0.9526			f2	0.9858	98.5871	0.9930
		f3	0.9075	90.7986	0.9538			f3	0.9783	97.8637	0.9893
	4 Layers	f1	0.9101	91.0442	0.9545		4 Layers	f1	0.9793	97.9311	0.9898
		f2	0.9193	91.9496	0.9589			f2	0.9817	98.1845	0.9909
		f3	0.9098	90.9871	0.9540			f3	0.9816	98.1651	0.9908

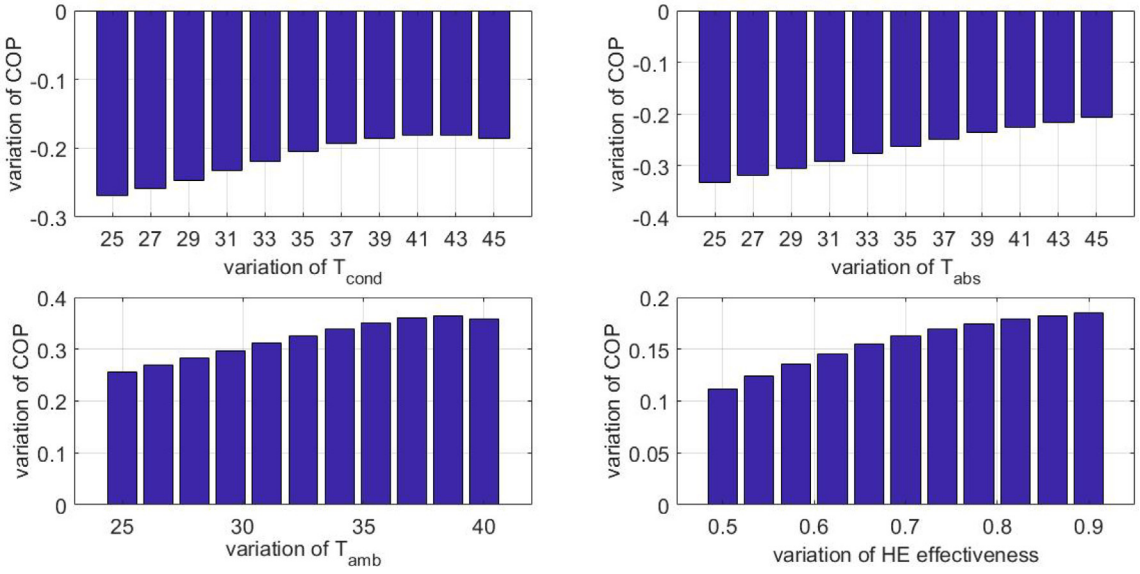

Fig. 12. Sensitivity analysis for the COP of the single-effect ACS.

optimum T_{gen} can be achieved by controlling the mass rate. As predicted by the sensitivity analyses and shown in Fig. 17, the T_{eva} of the optimized model varies slightly, in that the effects of the variation of the T_{amb} are balanced out by the variations of the T_{cond} and T_{abs}. Furthermore, the amount of T_{eva}, in this case, is about 1.6 °C greater than the result of Bellos et al. (2017).

Fig. 18 illustrates that the optimized model produced more cooling load (Q_{eva}) than the Bellos et al. model. The difference in the cooling loads between the two models is assumed to be compensated by the addition of an auxiliary heater. The difference between the two models before 12:00 is higher than after 12:00.

If an auxiliary heater makes up for the extra energy needed to achieve the optimized model Q_{eva}, the cost savings due to the reduction of the consumption of additional natural gas in the auxiliary heater would be 187 dollars per square meter of solar collector. In addition, the reduction of carbon dioxide emissions would be about 33.5 kg per square meter of solar collector (as shown in Table 8).

5. Conclusion

In this paper, the operational optimization of a single-effect absorption cooling system and the correlations to obtain the

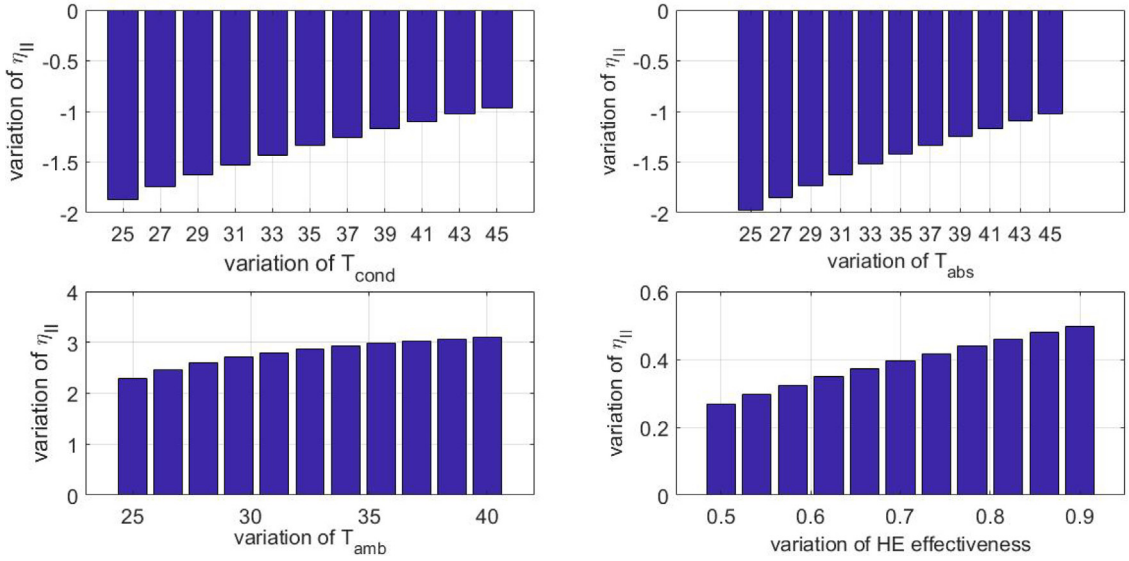

Fig. 13. Sensitivity analysis for the exergetic efficiency (η_π) of the single-effect ACS.

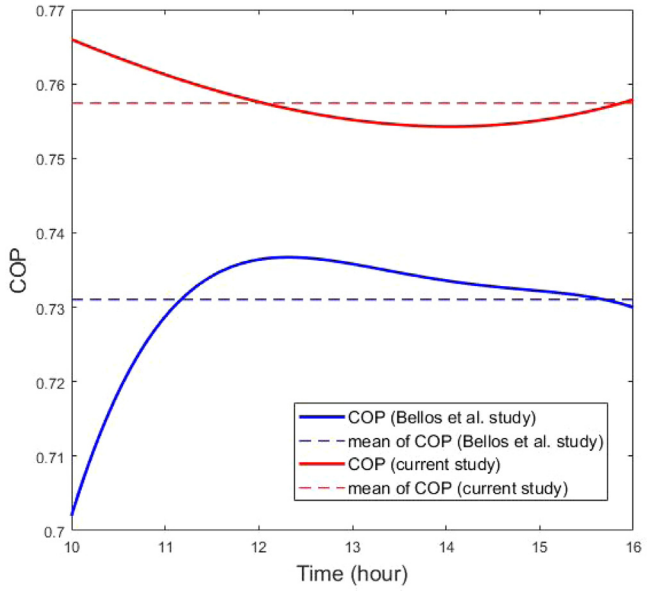

Fig. 14. Comparison between the COP of the ACS of Bellos et al. (2017) and the optimized one of this study.

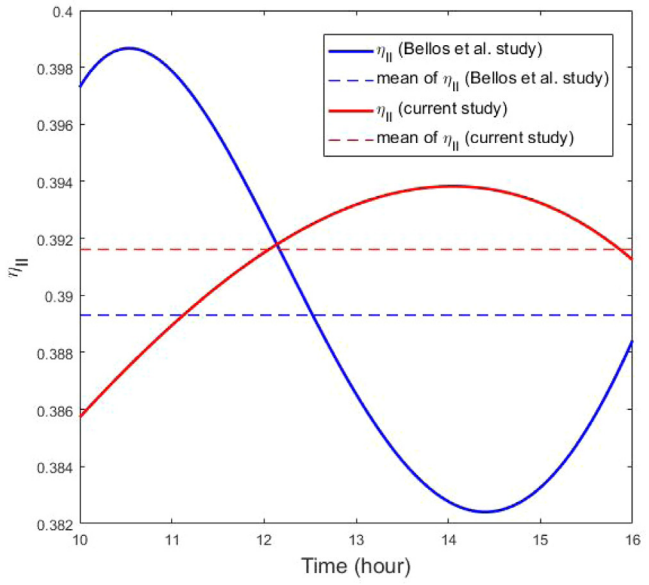

Fig. 15. Comparison between the η_Π of the ACS of Bellos et al. (2017) and the optimized one of this study.

Table 8
Relative reduction of cost savings and carbon dioxide emissions of (Bellos et al., 2017) and this study.

Carbon dioxide emission reduction	Cost-saving
33.5245 (kg/m^2_{col})	186.9608 ($\$/m^2_{col}$)

optimum mode of the system under defined operational conditions were presented and discussed. The system was modeled using MATLAB and a genetic algorithm and it was then optimized to maximize coefficient of performance and exergetic efficiency, by varying the generator and evaporator temperatures at a specific operational condition. By repeating this process for different operational conditions, a database for the coefficient of performance, exergetic efficiency, as well as generator and evaporator temperatures was created. In addition, the influence of operational conditions on outputs like the optimum generator and evaporator temperatures, the coefficient of performance, and exergetic efficiency were studied using the GMDH approach. The resulting correlations were found to be within proper ranges of different criteria.

Sensitivity analyses of the correlations illustrated that all operational parameters, except the effectiveness of the heat exchanger, had inverse influences on the optimum generator and evaporator temperatures. The effect of the condenser and absorber temperatures were almost analogous to each other. However, the most effective parameter to obtain the optimum evaporator temperature was found to be the ambient temperature. Finally, the optimum mode of the single-effect absorption cooling system was coupled with an evacuated tube solar collector and was compared to a similar but not an optimized system. The values obtained in the present study were compared with the corresponding values of Bellos et al. study. Considerable improvements in maximum values of energetic and exergetic efficiencies

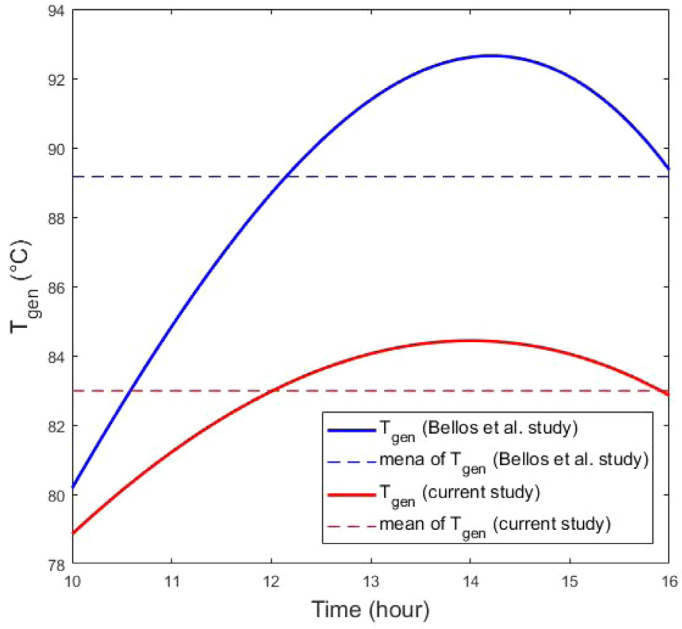

Fig. 16. Comparison between the T_{gen} of the ACS of Bellos et al. (2017) and the optimized one of this study.

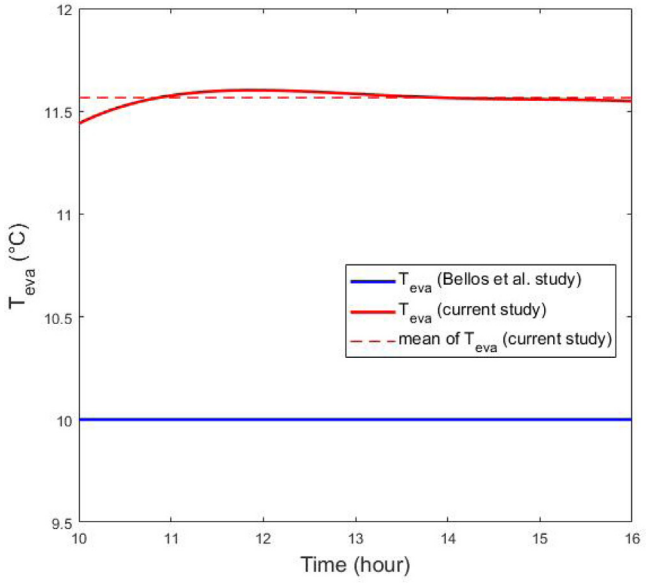

Fig. 17. Comparison between T_{eva} of the ACS of Bellos et al. (2017) and the optimized one of this study.

are 9.1% and 3.0, respectively. In addition, a significant general improvement in the energetic efficiency (3.6%) and a slight improvement in the exergetic efficiency (0.6%) were achieved by decreasing the mean temperature of the generator by about 6.2 °C and by increasing the mean temperature of the evaporator by about 1.6 °C. The observed improvement in exergetic efficiency is relatively small when compared to Bellos et al. study, as it was already optimized exergetically from the baseline. Accordingly, the optimum mode of the absorption cooling system brought about not only improvements in the thermodynamic performance but it also decreased the generator temperature. This is a significant result for the adoption and application of low-grade heat like solar energy. Furthermore, the higher performance of the optimized

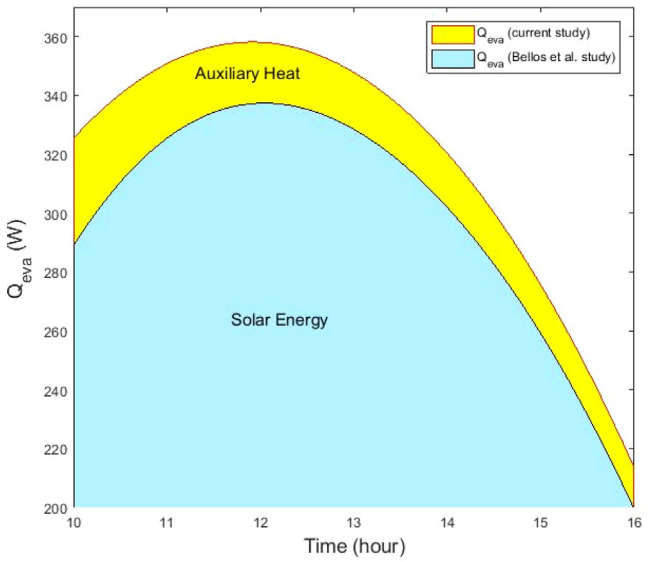

Fig. 18. Comparison between Q_{eva} per square meter solar collector of the ACS of Bellos et al. (2017) and the optimized one of this study.

system led to cost savings of 187 dollars per square meter of solar collector and a decrease in carbon dioxide emissions of about 33.5 kg per square meter of solar collector.

The present study was striving to find a model for the thermodynamic optimum mode of absorption cooling system with the goal of improving operational efficiency. Further research can explore the optimization of other aspects, like economics and environmental impacts, as well as examine other modeling methods.

CRediT authorship contribution statement

S. Sharifi: Conceptualization, Methodology, Software, Validation, Resources, Writing - original draft, Visualization. **F. Nozad Heravi:** Methodology, Software, Validation, Formal analysis, Resources, Writing - original draft. **R. Shirmohammadi:** Conceptualization, Methodology, Writing - review & editing. **R. Ghasempour:** Project administration, Supervision, Conceptualization, Resources, Writing - review & editing. **F. Petrakopoulou:** Conceptualization, Validation, Writing - review & editing. **L.M. Romeo:** Conceptualization, Writing - review & editing.

Declaration of competing interest

The authors declare that they have no known competing financial interests or personal relationships that could have appeared to influence the work reported in this paper.

Acknowledgments

The authors hereby acknowledge the department of Renewable Energies and Environment of University of Tehran for their scientific support and their proofreading of manuscript. The authors are also so grateful for the valuable comments of Editors and Reviewers for which enhanced the paper quality.

References

Ahmadi, M.H., Hosseinzade, H., Sayyaadi, H., Mohammadi, A.H., Kimiaghalam, F., 2013. Application of the multi-objective optimization method for designing a powered stirling heat engine: Design with maximized power thermal efficiency and minimized pressure loss. Renew. Energy 60, 313–322, https://doi.org/10.1016/j.renene.2013.05.005.

Ali, A.H.H., 2017. Performance-cost and global warming assessments of two residential scale solar cooling systems versus a conventional one in hot arid areas. Sustain. Energy Technol. Assessments 20, 1–8, https://doi.org/10.1016/j.seta.2017.01.006.

Ali, A.H.H., Noeres, P., Pollerberg, C., 2008. Performance assessment of an integrated free cooling and solar powered single-effect lithium bromide-water absorption chiller. Sol. Energy 82, 1021–1030, https://doi.org/10.1016/j.solener.2008.04.011.

Arora, J., 2012. Introduction To Optimum Design. Academic Press, https://doi.org/10.1016/C2009-0-61700-1.

Avanessian, T., Ameri, M., 2014. Energy, exergy, and economic analysis of single and double effect LiBr–H2O absorption chillers. Energy Build. 73, 26–36, https://doi.org/10.1016/J.ENBUILD.2014.01.013.

Azhar, M., Siddiqui, M.A., 2017. Energy and exergy analyses for optimization of the operating temperatures in double effect absorption cycle. Energy Procedia 109, 211–218, https://doi.org/10.1016/j.egypro.2017.03.043.

Bagheri, B.S., Shirmohammadi, R., Mahmoudi, S.M.S., Rosen, M.A., 2019. Optimization and comprehensive exergy-based analyses of a parallel flow double-effect water-lithium bromide absorption refrigeration system. Appl. Therm. Eng. 152, 643–653, https://doi.org/10.1016/j.applthermaleng.2019.02.105.

Bejan, A., Tsatsaronis, G., Moran, M., 1996. Thermal Design and Optimization. John Wiley and Sons. Wiley.

Bellos, E., Tzivanidis, C., Symeou, C., Antonopoulos, K.A., 2017. Energetic, exergetic and financial evaluation of a solar driven absorption chiller – a dynamic approach. Energy Convers. Manage. 137, 34–48, https://doi.org/10.1016/j.enconman.2017.01.041.

Besarati, S.M., Atashkari, K., Jamali, A., Hajiloo, A., Nariman-zadeh, N., 2010. Multi-objective thermodynamic optimization of combined brayton and inverse brayton cycles using genetic algorithms. Energy Convers. Manag. 51, 212–217, https://doi.org/10.1016/j.enconman.2009.09.015.

Chen, J.F., Dai, Y.J., Wang, R.Z., 2017. Experimental and analytical study on an air-cooled single effect LiBr-H2O absorption chiller driven by evacuated glass tube solar collector for cooling application in residential buildings. Sol. Energy 151, 110–118, https://doi.org/10.1016/j.solener.2017.05.029.

Şencan, A., Yakut, K.A., Kalogirou, S.A., 2005. Exergy analysis of lithium bromide/water absorption systems. Renew. Energy 30, 645–657, https://doi.org/10.1016/j.renene.2004.07.006.

Davarpanah, A., Shirmohammadi, R., Mirshekari, B., Aslani, A., 2019. Analysis of hydraulic fracturing techniques: hybrid fuzzy approaches. Arab. J. Geosci. https://doi.org/10.1007/s12517-019-4567-x.

Deb, K., Pratap, A., Agarwal, S., Meyarivan, T., 2002. A fast and elitist multiobjective genetic algorithm: NSGA-II. IEEE Trans. Evol. Comput. 6, 182–197, https://doi.org/10.1109/4235.996017.

Debnath, S., Reddy, M.M., Yi, Q.S., 2014. Environmental friendly cutting fluids and cooling techniques in machining: A review. J. Clean. Prod. 83, 33–47, https://doi.org/10.1016/j.jclepro.2014.07.071.

Dincer, I., Cengel, Y.A., 2001. Energy, entropy and exergy concepts and their roles in thermal engineering. Entropy 3, 116–149, https://doi.org/10.3390/e3030116.

Farlow, S.J., 1981. The gmdh algorithm of ivakhnenko. Am. Stat. 35, 210–215, https://doi.org/10.1080/00031305.1981.10479358.

Florides, G.A., Kalogirou, S.A., Tassou, S.A., Wrobel, L.C., 2003. Design and construction of a LiBr-water absorption machine. Energy Convers. Manag. 44, 2483–2508, https://doi.org/10.1016/S0196-8904(03)00006-2.

Fratzscher, W., 1997. The exergy method of thermal plant analysis. Int. J. Refrig. Butterworths, https://doi.org/10.1016/s0140-7007(97)85546-6.

Ghani, M.U., Zaman, M., Khan, I., 2017. Thermodynamic modeling and optimization of double effect series flow LiBr-H2O vapor absorption chiller. In: ICET 2016-2016 Int. Conf. Emerg. Technol. https://doi.org/10.1109/ICET.2016.7813266.

Ghorbani, B., Hamedi, M., Shirmohammadi, R., Mehrpooya, M., Hamedi, M.-H., 2016. A novel multi-hybrid model for estimating optimal viscosity correlations of Iranian crude oil. J. Pet. Sci. Eng. 142, https://doi.org/10.1016/j.petrol.2016.01.041.

Ghorbani, B., Shirmohammadi, R., Amidpour, M., Inzoli, F., Rocco, M., 2019. Design and thermoeconomic analysis of a multi-effect desalination unit equipped with a cryogenic refrigeration system. Energy Convers. Manag. https://doi.org/10.1016/j.enconman.2019.112208.

Ghorbani, B., Shirmohammadi, R., Mehrpooya, M., 2020. Development of an innovative cogeneration system for fresh water and power production by renewable energy using thermal energy storage system. Sustain. Energy Technol. Assessments https://doi.org/10.1016/j.seta.2019.100572.

Ghorbani, B., Shirmohammadi, R., Mehrpooya, M., Hamedi, M.H., 2018a. Structural, operational and economic optimization of cryogenic natural gas plant using NSGAII two-objective genetic algorithm. Energy 159, 410–428, https://doi.org/10.1016/j.energy.2018.06.078.

Ghorbani, B., Shirmohammadi, R., Mehrpooya, M., Mafi, M., 2018b. Applying an integrated trigeneration incorporating hybrid energy systems for natural gas liquefaction. Energy 149, 848–864, https://doi.org/10.1016/j.energy.2018.02.093.

Goldberg, D.E., David, E., 1989. Genetic algorithms in search, optimization, and machine learning. In: Choice Reviews Online. Addison-Wesley Longman Publishing Co. Inc, https://doi.org/10.5860/choice.27-0936.

Gomri, R., 2009. Second law comparison of single effect and double effect vapour absorption refrigeration systems. Energy Convers. Manage. 50, 1279–1287, https://doi.org/10.1016/j.enconman.2009.01.019.

Gomri, R., 2013a. Simulation study on the performance of solar / natural gas absorption cooling chillers. Energy Convers. Manage. 65, 675–681, https://doi.org/10.1016/j.enconman.2011.10.030.

Gomri, R., 2013b. Simulation study on the performance of solar/natural gas absorption cooling chillers. Energy Convers. Manage. 65, 675–681, https://doi.org/10.1016/j.enconman.2011.10.030.

Izquierdo, M., González-Gil, A., Palacios, E., 2014. Solar-powered single-and double-effect directly air-cooled LiBr-H2O absorption prototype built as a single unit. Appl. Energy 130, 7–19, https://doi.org/10.1016/j.apenergy.2014.05.028.

Jafarian, H., Sayyaadi, H., Torabi, F., 2017. Modeling and optimization of dew-point evaporative coolers based on a developed GMDH-type neural network. Energy Convers. Manage. 143, 49–65, https://doi.org/10.1016/j.enconman.2017.03.015.

Kalogirou, S., 2003. The potential of solar industrial process heat applications. Appl. Energy 76, 337–361, https://doi.org/10.1016/S0306-2619(02)00176-9.

Kaushik, S.C., Arora, A., 2009. Energy and exergy analysis of single effect and series flow double effect water-lithium bromide absorption refrigeration systems. Int. J. Refrig. 32, 1247–1258, https://doi.org/10.1016/j.ijrefrig.2009.01.017.

Kaynakli, O., Kilic, M., 2007. Theoretical study on the effect of operating conditions on performance of absorption refrigeration system. Energy Convers. Manage. 48, 599–607, https://doi.org/10.1016/j.enconman.2006.06.005.

Kholghi, S.A., Mahmoudi, S.M.S., 2019. Energy and exergy analysis of a modified absorption cycle: A comparative study. Sustain. Energy Technol. Assessments 32, 19–28, https://doi.org/10.1016/j.seta.2019.01.002.

Kilic, M., Kaynakli, O., 2007. Second law-based thermodynamic analysis of water-lithium bromide absorption refrigeration system. Energy 32, 1505–1512, https://doi.org/10.1016/j.energy.2006.09.003.

Klomfar, J., Pa, J., 2009. Short communication a simple formulation for thermodynamic properties of steam from 273 to 523 K, explicit in temperature and pressure's de la vapeur d ' eau une formulation simple pour les proprie' cision de la tempe' rature et la entre 273 et 523 K. Int. J. Refrig. 32, 1123–1125, https://doi.org/10.1016/j.ijrefrig.2008.12.010.

Kumar, A., Layek, A., 2019. Energetic and exergetic performance evaluation of solar air heater with twisted rib roughness on absorber plate. J. Clean. Prod. 232, 617–628, https://doi.org/10.1016/j.jclepro.2019.05.363.

Medjo Nouadje, B.A., Ngouateu Wouagfack, P.A., Tchinda, R., 2016. Finite-time thermodynamics optimization of an irreversible parallel flow double-effect absorption refrigerator. Int. J. Refrig. 67, 433–444, https://doi.org/10.1016/j.ijrefrig.2016.02.014.

Mehrpooya, M., Taromi, M., Ghorbani, B., 2019. Thermo-economic assessment and retrofitting of an existing electrical power plant with solar energy under different operational modes and part load conditions. Energy Reports. https://doi.org/10.1016/j.egyr.2019.07.014.

Misenheimer, C.T., Terry, S.D., 2017. The development of a dynamic single effect, lithium bromide absorption chiller model with enhanced generator fidelity. Energy Convers. Manage. 150, 574–587, https://doi.org/10.1016/j.enconman.2017.08.005.

Misra, R.D., Sahoo, P.K., Gupta, A., 2006. Thermoeconomic evaluation and optimization of an aqua-ammonia vapour-absorption refrigeration system. Int. J. Refrig. 29, 47–59, https://doi.org/10.1016/j.ijrefrig.2005.05.015.

Modi, B., Mudgal, A., Patel, B., 2017. Energy and exergy investigation of small capacity single effect lithium bromide absorption refrigeration system. Energy Procedia 109, 203–210, https://doi.org/10.1016/j.egypro.2017.03.040.

Nasruddin, Sholahudin, Satrio, P., Mahlia, T.M.I., Giannetti, N., Saito, K., 2019. Optimization of HVAC system energy consumption in a building using artificial neural network and multi-objective genetic algorithm. Sustain. Energy Technol. Assessments 35, 48–57, https://doi.org/10.1016/j.seta.2019.06.002.

Pandya, B., Patel, J., Mudgal, A., 2017. Thermodynamic evaluation of generator temperature in libr-water absorption system for optimal performance. Energy Procedia 109, 270–278, https://doi.org/10.1016/j.egypro.2017.03.063.

Pátek, J., Klomfar, J., 2006. A computationally effective formulation of the thermodynamic properties of LiBr-H2O solutions from 273 to 500 K over full composition range. Int. J. Refrig. 29, 566–578, https://doi.org/10.1016/j.ijrefrig.2005.10.007.

Petela, K., Manfrida, G., Szlek, A., 2017. Advantages of variable driving temperature in solar absorption chiller. Renew. Energy 114, 716–724, https://doi.org/10.1016/j.renene.2017.07.060.

Petrakopoulou, F., Tsatsaronis, G., Morosuk, T., 2012a. Advanced exergoenvironmental analysis of a near-zero emission power plant with chemical looping combustion. Environ. Sci. Technol. 46, 3001–3007, https://doi.org/10.1021/es203430b.

Petrakopoulou, F., Tsatsaronis, G., Morosuk, T., Carassai, A., 2012b. Conventional and advanced exergetic analyses applied to a combined cycle power plant. Energy 41, 146–152, https://doi.org/10.1016/j.energy.2011.05.028.

Romeo, L.M., Gareta, R., 2006. Neural network for evaluating boiler behaviour. Appl. Therm. Eng. 26, 1530–1536, https://doi.org/10.1016/j.applthermaleng.2005.12.006.

Samanta, S., Basu, D.N., 2016. Energy and entropy-based optimization of a single-stage water-lithium bromide absorption refrigeration system. Heat Transf. Eng. 37, 232–241, https://doi.org/10.1080/01457632.2015.1044420.

Saravanan, R., Maiya, M.P., 1998. Thermodynamic comparison of water-based working fluid combinations for a vapour absorption refrigeration system. Appl. Therm. Eng. 18, 553–568, https://doi.org/10.1016/S1359-4311(97)00072-0.

Seshadri, K., 1996. Thermal design and optimization. In: Energy. Wiley, https://doi.org/10.1016/s0360-5442(96)90000-6.

Shirazi, A., Taylor, R.A., White, S.D., Morrison, G.L., 2016. Transient simulation and parametric study of solar-assisted heating and cooling absorption systems: An energetic, economic and environmental (3E) assessment. Renew. Energy 86, 955–971, https://doi.org/10.1016/j.renene.2015.09.014.

Shirmohammadi, R., Ghorbani, B., Hamedi, M., Hamedi, M.H., Romeo, L.M., 2015. Optimization of mixed refrigerant systems in low temperature applications by means of group method of data handling (GMDH). J. Nat. Gas Sci. Eng. 26, 303–312, https://doi.org/10.1016/j.jngse.2015.06.028.

Shirmohammadi, R., Soltanieh, M., Romeo, L.M., 2018. Thermoeconomic analysis and optimization of post-combustion CO2 recovery unit utilizing absorption refrigeration system for a natural-gas-fired power plant. Environ. Prog. Sustain. Energy 37, 1075–1084, https://doi.org/10.1002/ep.12866.

Sokhansefat, T., Kasaeian, A., Rahmani, K., Heidari, A.H., Aghakhani, F., Mahian, O., 2018. Thermoeconomic and environmental analysis of solar flat plate and evacuated tube collectors in cold climatic conditions. Renew. Energy 115, 501–508, https://doi.org/10.1016/j.renene.2017.08.057.

Teng, G., Xiao, J., He, Y., Zheng, T., He, C., 2017. Use of group method of data handling for transport energy demand modeling. Energy Sci. Eng. 5, 302–317, https://doi.org/10.1002/ese3.176.

Xu, D., Qu, M., Hang, Y., Zhao, F., 2015. Multi-objective optimal design of a solar absorption cooling and heating system under life-cycle uncertainties. Sustain. Energy Technol. Assessments 11, 92–105, https://doi.org/10.1016/j.seta.2015.07.001.

Ziari, H., Sobhani, J., Ayoubinejad, J., Hartmann, T., 2015. Prediction of IRI in short and long terms for flexible pavements: ANN and GMDH methods. Int. J. Pavement Eng. 17, 776–788, https://doi.org/10.1080/10298436.2015.1019498.